The Meteoritical Society

Meteoritics & Planetary Science 1–13 (2020)
doi: 10.1111/maps.13573-3267

Check for updates

Electronic-Only Article

A novel geomatics method for assessing the Haughton impact structure

Calder W. PATTERSON* and Richard E. ERNST

Department of Earth Sciences, Ottawa Carleton Geoscience Center, Carleton University, 1125 Colonel By Drive, Ottawa, Ontario K1S 5B6, Canada
*Corresponding author. E-mail: calderpatterson@cmail.carleton.ca

(Received 22 July 2019; revision accepted 22 August 2020)

Abstract–Terrestrial impact structures are typically modified by erosion, burial, and tectonic deformation. Their systematic morphologies are typically reconstructed through a combination of geological and topographic mapping, satellite imagery, and geophysical surveys. This study applies a novel geomatics approach to assessment of the morphology of the extensively studied Haughton impact structure (HIS), Devon Island, Nunavut, in order to test its potential to improve the accuracy and quality of future impact structure reconstruction. This new methodology integrates HIS lithological data, in the form of digitized geologic mapping, with a digital elevation model, within diametrically opposed, wedge-shaped couplets, and plots these data as pseudo cross sections that capitalize on the radial symmetry of the impact structure. The pseudo cross sections provide an accurate reconstruction of the near-surface stratigraphic sequences and terraces in the faulted annulus of the modified crater rim. The resultant pseudo cross sections support current interpretations regarding the 10–12 km diameter of the transient cavity, and successfully reproduce the visible outer ring and intermediate uplifted zone within the central basin. Observed positions of vertical offsets suggest that the extent of impact deformation extends beyond the current estimates of the apparent crater rim to radial distances of between 14 and 15 km. Finally, the new geomatics approach provides an improved determination of the spatial, stratigraphic, and temporal relationships among the Haughton Formation lake sediments, allochthonous crater-fill impactites, and uplifted target rocks, and indicates that there was a not-insignificant time gap between the formation of the impact structure and the deposition of the sediments.

INTRODUCTION

Impact cratering is a common and fundamental process for the active reshaping of the surfaces of all rocky celestial bodies. Impact structures form when hypervelocity impactors of varying size strike the surface of a larger celestial body. On Earth, the ongoing processes of erosion and tectonism modify impact structures as they may be buried by sediment, become partially to completely eroded away, and/or be deformed by postimpact tectonic processes. Due to the fundamental processes associated with the formation of impact craters, the interpretation of the observed morphology and state of preservation can be important factors for determination of a planet's geologic history (Dence 1972; Grieve 1981; Osinski and Spray 2005).

The Haughton impact structure (HIS) is a complex crater located on Devon Island, Nunavut, Canada (Fig. 1). The impact structure has been dated using distinct isotope methods at ~39 Ma (Sherlock et al. 2005) and ~23.5 Ma (Young et al. 2013). While some of the original near-surface materials associated with the crater have been eroded away, a striking assemblage of geological and geophysical features is retained within its distinctive target stratigraphy. For decades, field data have been collected from the HIS, including a near-radial seismic line (Scott and Hajnal 1988), gravity and magnetic field measurements (Pohl et al. 1988), and detailed geological mapping (Robertson and Sweeney 1983; Bischoff and Oskierski 1988; Osinski et al. 2005a). The HIS target rocks comprise ~1880 m of westward

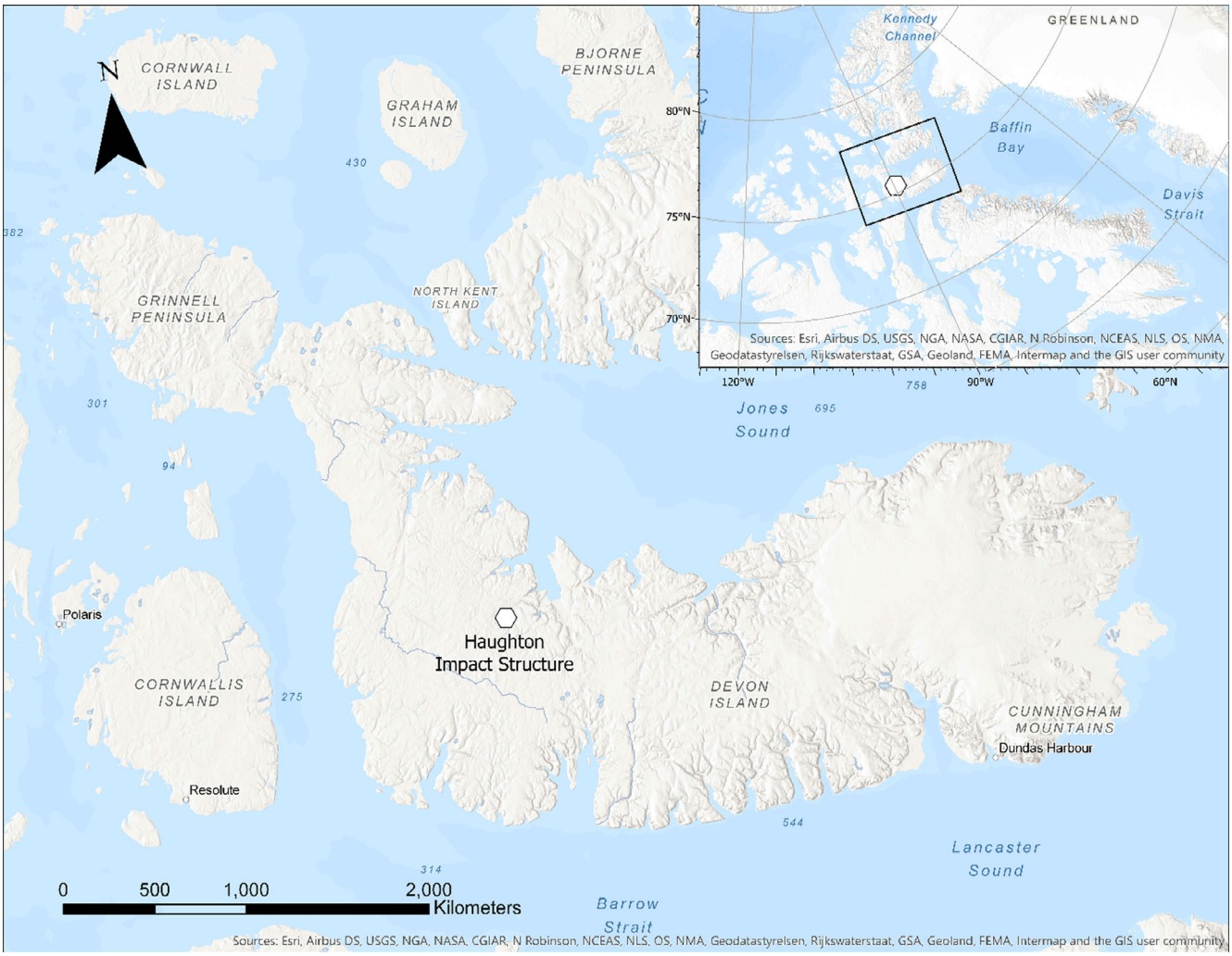

Fig. 1. Location map showing the position of the Haughton impact structure (Hexagon; 75°22′38″N, 89°40′48″W) on Devon Island in Nunavut, Canadian Arctic (map extent, inset).

dipping (2–5°) Paleozoic carbonates overlying crystalline basement (Grieve 1988). An extensive impact-derived melt-bearing breccia unit fills the crater center, but isolated outcrops outside of this area suggest that the crater-fill impact melt rocks originally covered a significantly larger area (Redeker and Stöffler 1988; Osinski et al. 2005b). The most recent interpretations of the HIS morphology by Osinski et al. (2005a) suggest a 10–12 km diameter transient cavity, a 16 km final crater rim diameter, a 23 km apparent crater diameter, and the lack of a central peak structure within the central uplift that protruded from pre-erosional crater-fill impact melt rocks. The wealth of previous studies carried out on the HIS provides a unique opportunity to evaluate novel analytical techniques for their potential to enhance our understanding of the origin and subsequent geologic history of the HIS and similar hypervelocity impact craters.

The goal of this study is to use modern geomatics geographic information system (GIS) analytics to test and refine previous conclusions regarding the size and morphology of the HIS, and to ultimately answer the following questions:

1. Can modern GIS methods be used to reconstruct or approximate the pre-erosional surface of young terrestrial impact structures?
2. If so, can GIS methods improve upon existing interpretations of a well-studied impact structure like the HIS?

GEOLOGICAL SETTING

History of Haughton Investigations

The circular HIS was originally recognized by Greiner in 1955 (Greiner 1963). At the time, few impact

structures were recognized, and complex crater morphologies were as yet poorly understood, so HIS was originally reported as a salt dome due to the pronounced central uplift of the feature (Greiner 1963; Robertson 1988). Based on its ~400 km geographic separation from other salt domes in the Sverdrup Basin and its shallow basin structure revealed by later regional topographic mapping, Dence (1965) proposed that it might be an impact structure. With the discovery of shatter cones (Robertson and Mason 1975) and coesite (Frisch and Thorsteinsson 1978), the impact origin of the Haughton structure was confirmed. Initial investigations concluded that the feature had a diameter of 16 km with a central uplift, and formed sometime during the Miocene to Pliocene, based on paleontological evidence from lake sediments that filled the basin shortly after the impact event (Frisch and Thorsteinsson 1978).

Further mapping and sampling (Robertson and Grieve 1978; Robertson and Sweeney 1983), as well as studies of shock metamorphism by Robertson and Plant (1981), led to a reassessment of the impact crater's size and morphology. The HIS was interpreted to comprise a three-ring system with an outer annulus of 20.5 km diameter; a middle ring of 14–15 km diameter; and an inner, elliptical ring of 3.5–5.5 km diameter. This assessment was determined using a terrestrial sedimentary-target scaling of lunar impact structures, with the HIS being identified as a complex crater, intermediate in size between a peak-ring basin and a multi-ring basin (Robertson and Sweeney 1983). Geophysical surveys also identified a concentric −11 mGal Bouguer gravity anomaly with a diameter of ~25 km (Todd 1979), and a 300 nT magnetic anomaly at the center of the structure with a diameter of ~3 km (Robertson and Sweeney 1983). These anomalies could not be explained based on analysis of the surface structures and were attributed to shallowly buried, highly shocked material.

The Haughton Impact Structure Study (HISS) of 1984 continued to investigate the geology of the site, resulting in a series of landmark publications (Grieve 1988). These included studies of surface structures (Bischoff and Oskierski 1988); seismic, gravity, and magnetic surveys (Pohl et al. 1988; Scott and Hajnal 1988); and geochemical analyses of impactites (Metzler et al. 1988; Redeker and Stöffler 1988). Fission-track age dating of apatites (Omar et al. 1987) and ^{40}Ar-^{39}Ar analysis of shocked gneisses (Jessberger 1988) yielded similar ages for the impact event at 23.4 ± 1.0 Ma and 22.4 ± 1.4 Ma, respectively. Investigation of the lacustrine sediments comprising the Haughton Formation suggests late-stage subsidence of the impact structure center, which caused the originally horizontal sediments to dip inward (Hickey et al. 1988). Another series of field studies, beginning in the late 1990s, focused on the state of shock metamorphism in the basement crystalline rocks, the morphology of the impact structure (Sharpton et al. 1998; Sharpton 1999), and potential of the site as an analog for Martian terrains (Lee et al. 1998; Zent et al. 1998).

Field mapping by Osinski (2005) produced the most detailed geological map of the impact structure, and the results presented in Osinski et al. (2005a, 2005b) present the most widely accepted interpretation regarding its size, morphology, and identification of contained complex tectonic structures (Osinski and Spray 2005). Dating of shocked clasts by Sherlock et al. (2005), using a more reliable combination of step heating and laser probe spot dating Ar/Ar analysis methods, revealed an Eocene age of impact (~39 Ma). The results of the latter study are considered to be more reliable than previous studies as the technique is less susceptible to age skewing by hydrothermal alteration and argon loss (Sherlock et al. 2005). Even more recently, Young et al. (2013) used radiogenic ^{4}He-based thermochronometers to obtain an Oligocene (~23.5 Ma; U-Th)/He date in zircon, which is resistant to disturbance by postimpact thermal events. Interesting work has also been conducted to study microbe–water–rock interactions in impact-generated hydrothermal alteration assemblages of the HIS as analogs for the habitability of Martian systems (Parnell et al. 2004; Izawa et al. 2011; Greenberger et al. 2016). Another study, by Osinski and Ferrière (2016), of the HIS shatter cones demonstrated that their distribution is an indicator of the extent of the apparent crater diameter and obliquity of the impact, and that they play a role in reducing the strength of target rocks, thus enhancing crater collapse. Further studies of the HIS investigated the central positive magnetic anomaly (~900 nT), and concluded that impact-generated hydrothermal alteration crystallized magnetite in the uplifted basement rock, which was subsequently concentrated in the near surface, producing the very strong anomaly observed presently (Quesnel et al. 2013; Zylberman et al. 2017).

Target Stratigraphy

The target stratigraphy of the HIS (Fig. 2) comprises ~1880 m of Proterozoic to Paleogene sedimentary rocks unconformably overlying a crystalline basement (Frisch and Thorsteinsson 1978; Osinski et al. 2005a). The Archean metamorphic basement is composed mainly of tonalitic to granitic gneisses of the Canadian Shield that outcrop along the coast in the eastern end of Devon Island, where they are overlain by the Devon Island Ice Cap (Osinski et al. 2005a). The

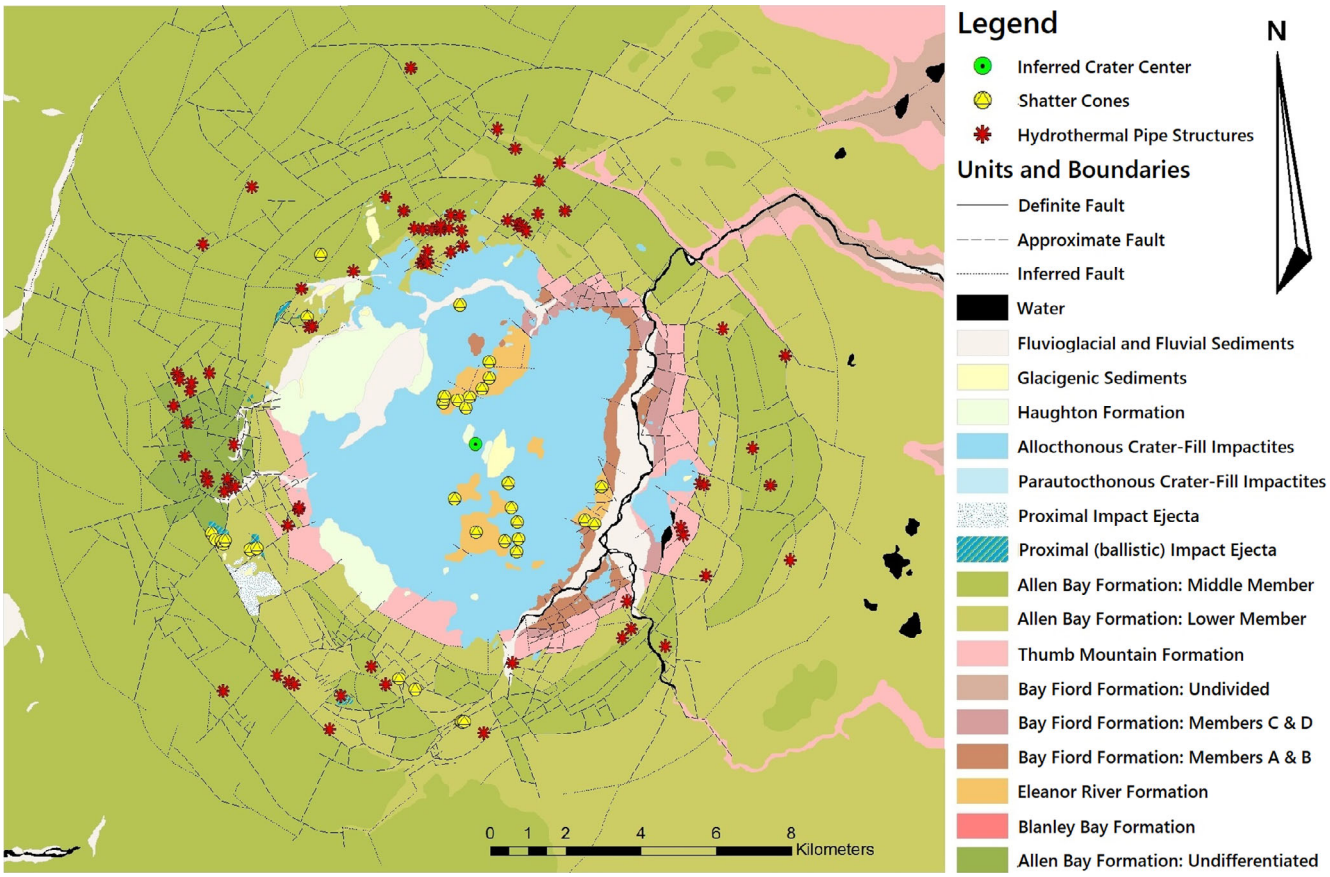

Fig. 2. Digitized product modified after the Geologic Map of the Haughton impact structure on Devon Island, Nunavut, Canada, by Osinski (2005). The crater center is at 75°22′38″N, 89°40′48″W.

Lower Paleozoic (Cambrian to Silurian) sedimentary sequence is dominated by thick units of limestone and dolomite that are generally undeformed except for a gentle 2–5° westward dip (Frisch and Thorsteinsson 1978; Thorsteinsson and Mayr 1987; Osinski et al. 2005a). The base of this sequence is comprised of Cambrian–Ordovician sedimentary units that do not outcrop within the impact structure itself, including the Rabbit Point and Bear Point formations, ~70 m inclusive (Thorsteinsson and Mayr 1987; Osinski et al. 2005a). Overlying these base units are two more lithologies that are not observed within the impact structure but are part of the original target stratigraphy: the Cass Fiord Formation (~250 m), which spans the remainder of the base Cambrian sedimentary sequence, and, with the overlying Cape Clay Formation (~80 m), makes up the lower ~100 m of the Ordovician sedimentary sequence (Thorsteinsson and Mayr 1987; Osinski et al. 2005a).

Ordovician–Silurian sedimentary successions that do outcrop within the structure from the oldest to youngest include ~185 m of alternating anhydrite and gypsum, dolomite, and limestone units belonging to the Blanley Bay Formation; 260 m of a thick limestone succession of the Eleanor River Formation; 290 m of anhydrite, gypsum, and dolomite belonging to the Bay Fiord Formation, which is divided into its lower A and B members and upper C and D members; 110 m of Thumb Mountain Formation limestone; 15 m of the Irene Bay Formation limestone; and the Allen Bay Formation, which is divided into a lower limestone member, and middle and upper dolomite members (Frisch and Thorsteinsson 1978; Thorsteinsson and Mayr 1987; Osinski et al. 2005a). Hickey et al. (1988) proposed that the original target stratigraphy also included more than 200 m of the siliciclastic-dominated Eureka Sound Formation, which is preserved in a nearby graben structure. This addition would increase the potential thickness of the target stratigraphy to approximately 2100 m. However, detailed geological mapping by Osinski (2005) did not reveal any evidence of this Eureka formation having been preserved in

downfaulted blocks of the HIS and these researchers concluded that this formation had been removed from the target prior to the impact event. Hence, the best estimate of the thickness of the target strata remains at 1880 m (Hajnal et al. 1988; Osinki et al. 2005a).

Site Geology and Structural Interpretations

Current structural interpretations were synthesized as part of the Haughton–Mars Project, and summarized by Osinski et al. (2005a). The apparent crater diameter is ~23 km, based on the outermost observed semicontinuous circumferential faults, and that the transient cavity diameter, equal to the excavation diameter (Grieve et al. 1981; Turtle et al. 2005), is estimated at ~10–12 km, as indicated by the presence of uplifted megablocks of excavated lithologies (Osinski et al. 2005a). Three primary structural regions were identified (Robertson and Sweeney 1983; Osinski et al. 2005a) as (1) a central basin, which occupies the same radial dimensions suggested for the transient cavity (radius of 5–6.5 km); (2) the rim (final crater), with a radius of approximately 8 km that is marked by the greatest vertical offsets (>50 m) of faulted terraces such that downdropped megablocks would not be completely obscured by an uneroded ejecta blanket (Grieve et al. 1981; Turtle et al. 2005); and (3) an outer region of faulted terraces that extend outward to a radius of 11–12 km from the crater center. Within the central basin, there are three subzones including an outer ring of uplifted (from depths of 250–750 m), faulted, subvertical to overturned strata at a radial distance between 5.0 and 6.5 km; an intermediate zone of kilometer-scale uplifted megablocks (from depths up to ~1300 m); and a 2 km in diameter core of deep uplifted megablocks (from depths up to ~1450 m depths). Osinski and Spray (2005) concluded that there is no central peak structure because the central uplifted material would not have protruded from the uneroded crater-fill melt rocks, which is a requirement to qualify as a central peak structure.

Since its formation, the HIS has been modified by complex erosional and depositional processes that have obscured surface features by removal of significant portions of ejecta and crater-fill impact melt rocks, and fault-channeled incising of valleys forming broad circumferential and radial valleys (Fig. 3). Postimpact units include the approximately 22–24 Ma Haughton Formation lake sediments (Frisch and Thorsteinsson 1978), and fluvial and glacial deposits that nonuniformly overlie large parts of the impact structure. To this day, several rivers flow through the structure and shallow lakes and ponds are found within the structure and throughout Devon Island (Table 1).

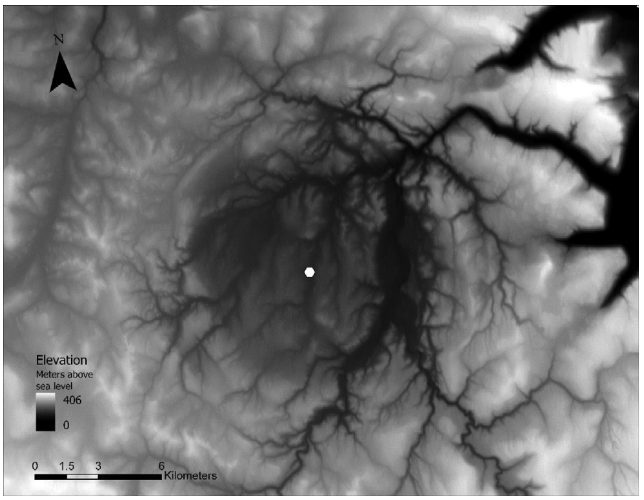

Fig. 3. This 20 m resolution digital elevation model was extracted from the Canadian Digital Elevation Model using the Government of Canada's (n.d.) Geospatial Data Extraction tool. The white hexagon is the interpreted crater center, at 75°22′38″N, 89°40′48″W.

METHODOLOGY

Conventional cross sections of terrestrial structures are excellent for illustrating the overall crater structure and distribution of lithologies at depth. For example, structural data can be used in concert with numerical models to produce cross sections that estimate the amount of erosion that an impact structure has undergone, as demonstrated by Kenkmann et al. (2005) in a study of the Upheaval Dome impact crater, Utah. However, these methods are limited in their usefulness for assessing how structures might have appeared before degradation by erosion because they may not be sufficiently quantitative to produce precise and unique estimates. We hope to overcome these limitations by using a novel approach for assessing the HIS that exclusively integrates observation-based geological data with a simple digital elevation model. This new method is presented herein that analyzes radially oriented, wedge-shaped areas to identify relationships between key structural and lithological features that constrain the original surface shape of the crater. This method capitalizes on the circular symmetry of impact structures and nonuniform erosion that results in concentrated incising of the impact structure, exposing buried structures and leaving original surface features between the incised areas. The angular sampling area juxtaposes geospatial and geological information that would otherwise be physically separated. The approach produces a spectrum of elevation data that can be combined with lithological data to make an image of the original surface and subsurface structures in the

Table 1. Summary of relevant structures described by Osinski et al. (2005a).

	Distance to crater center	Structural aspects
Central basin		
Inner core	~2 km (diameter)	Very deep uplifted blocks (~1450 m deep); subvertical to overturned
Intermediate zone	1.0–5.0 km	Deep uplifted (~1 km scale) megablocks (~1300 m deep)
Non-peak central uplift	N/A	The central uplift did not originally protrude from the crater-fill impactite lens
Outer ring	5.0–6.5 km	Uplifted, rotated, excavated strata (from 250 to 750 m deep)
Faulted annulus		
Faulted terraces	6–12 km	Up and out stepping fault-bounded megablocks
Final crater rim	~8 km	Innermost limit of megablocks not obscured by ejecta (>50 m fault offsets)
Apparent crater rim	11–12 km	Outermost semicontinuous normal fault

form of pseudo cross sections. To do this, the following steps were implemented.

1. Published geologic maps (Fig. 2; Osinski 2005) were georeferenced and digitized as polygons, and subsequently classified by their stratigraphic formations.
2. A 20 m resolution digital elevation model was extracted from the Canadian Digital Elevation Model using the Government of Canada's (n.d.) Geospatial Data Extraction tool (Fig. 3).
3. A fixed crater center was constrained at 75°22′38″N, 89°40′48″W based on its geometric positioning, the central topographic low, and a low Bouguer anomaly (Pohl et al. 1988).
4. The straight line radial distance from the crater center and angular position with respect to the crater center were calculated for each pixel in the digital elevation model.
5. The lithologies from the digitized geologic map were joined to the digital elevation model based on their geospatial location. For each pixel in the DEM, in addition to elevation value, there is also a radial distance from the crater center, an angular position with respect to the crater center, and a lithological identity.
6. The complete DEM data set was then analyzed to produce wedge-shaped area subsets around the crater center. For example, to create a pair of diametrically opposed wedges with arc lengths of 90° to the west and east of the crater center, a query was made to extract all pixels with angular positions between S45°W and N45°W for the western wedge area, and pixels with angular positions between S45°E and N45°E for the eastern wedge area. The orientation of each couplet can be adjusted in any direction to cross any features of interest. This study focuses couplets oriented from west to east so that the pseudo cross section is perpendicular to the strike of the regional westward dip of the target strata.
7. Once the desired subsets of pixels were extracted, they could be plotted as a pseudo cross section that followed a central ray within the wedge, based on the calculated distance from the crater center. The radial position of the crater center was defined as 25,000 m. To generate sections that spanned the entire structure, diametrically opposed couplets were generated by calculating the radial position of the pixels differently depending on the wedge area in question. The radial position of pixels within the western wedge areas was calculated by subtracting the distance from the crater center from 25,000 m, and the radial position of pixels within the eastern wedge area was calculated by adding the distance from the crater center to 25,000 m. Just like in any cross section, the elevation component of each pixel was plotted as the vertical component of the graph.
8. Lithological associations of each pixel were illustrated by assigning colors that relate to the digitized geological mapping color scheme.

Display Priority

The pseudo cross sections were given a 50:1 vertical exaggeration with respect to the radial position to emphasize variations in the elevation profiles across the 50 km long sections. The lithological color scheme employed in this study differed from the original mapping colors of Osinski (2005) to improve the discernibility of units within the pseudo cross sections.

The presence of a number of non-relevant lithologies and features in association with the HIS (e.g., postimpact fluvial, glacial sediments, water) complicates interpretation of structures pertaining to the original impact crater. One benefit of these features, however, is that they delineate where there are valleys cross-cutting the sampled wedge areas, since these features are mostly obscured by the juxtaposition of neighboring outcrops. Since fluvial and glacial sediments typically accumulate along the floor of incised

valleys, they can be used to determine whether structures observed in the pseudo sections should be interpreted as impact-related or erosion-derived.

After making note of the position and orientations of the fluvial and glacial sediments, they were removed from subsequent sections so as not to obscure structures of interest. The Haughton Formation was retained because of its significance to the sedimentary history of the structure as a postimpact crater-filling lithology. Also removed from consideration were the impact ejecta and parautochthonous impactites, which do not cover significant enough areas to be of use in interpreting large-scale structures, which is the main focus of this study. The more substantive main crater-filling allochthonous impactites were retained.

Display order refers to the order that geological units are drawn in pseudo cross sections, units drawn in the foreground overlay units drawn in the background from the perspective of the viewer. The foreground display order of the sedimentary target units was by order of stratigraphic succession, with the uppermost stratigraphic unit (i.e., Middle Allen Bay Formation) having the lowest display priority and the deepest stratigraphic unit (i.e., Blanley Bay Formation) having the highest display priority. This ordering was done to maximize the visibility of all units included in the structure. The display order of the Haughton Formation and the allochthonous crater-fill impactites were done differently and assigned the lowest and second lowest display priority, respectively, so that target stratigraphy units within the central area of the structure were not obscured.

RESULTS

Three series of diametrically opposed, wedge area couplets plotted as pseudo cross sections were produced, each covering the entire HIS using wedge areas with arc lengths of 90°, 45°, and 30°. Annotated examples are presented of 90° pseudo cross sections (Figs. 4 and 5). All pseudo cross sections produced with arc lengths of 90°, 45°, and 30° have been included as supplementary figures in supporting information.

The most significant difference between the different wedge area arc lengths is simply the number of data points included in the plots, where larger areas (especially 90°) capture more pixels in a wedge compared to smaller areas. Therefore, a more robust section is produced from larger wedge areas, but the trade-off is that there is greater uncertainty regarding the lateral spatial relationships within the larger areas. At first glance, the smaller wedge areas demonstrate fewer observable features. However, when the entire 30° series is analyzed as a whole, discrete structural features can be identified with a greater certainty that they are true representations of the impact structure. This is explained by Tobler's first law of geography, whereby objects that are closer together are more related than those that are far apart (Tobler 1970). While the larger wedge area sections visually appear more robust, they are actually better suited for summarizing features that are observed in the smaller wedge area sections. An exception to this is in the near-center components of the crater, where large arc length separations do not translate to large geographic distances.

Stratigraphic Reconstruction

Topographically, the study area is comprised of deeply incised valleys formed by fluvial erosion that often follows radial or circumferential paths, likely channeled by impact-related faults. The deepest of these channels is observed to the north and east of the crater center, producing the greatest range of topographic profiles, from sea level to ~380 m above sea level. With conventional mapping, these erosional features normally complicate assessment of original (pre-erosional) structures. However, in the nearly flat-lying and relatively undeformed sedimentary target of the HIS, these deep channels often expose buried stratigraphy. Their surface expressions are reduced by juxtaposed neighboring data in the pseudo cross sections. Thus, the pseudo cross sections simultaneously restore surface features and display buried stratigraphic successions in the distal areas of the modified crater (Fig. 5). The results are a testament to the excellent quality of the geological mapping as a geospatial data set such that it can be effectively joined with other geospatial data, in this case a digital elevation model.

Terraces and the Regional Plateau

An additional significant topographic effect is the nonuniform elevation of the regional plateau, which in most sections is between 350 and 380 m above sea level. In sections that pass over the northwest section the study area is only ~250 m above sea level and is reached at a shorter radius from the crater center than in other quadrants. It is unclear whether this difference in elevation is a result of nonuniform erosion due to ocean-ward drainage patterns that evenly eroded the surface of strata to the northwest, while deeply incising the same strata to the north, south, and east, or if this is an original characteristic of the target stratigraphy. Both hypotheses have significant and different implications for interpretation of the original HIS morphology. If the difference in elevation is a result of nonuniform postimpact erosion, then these deep incised

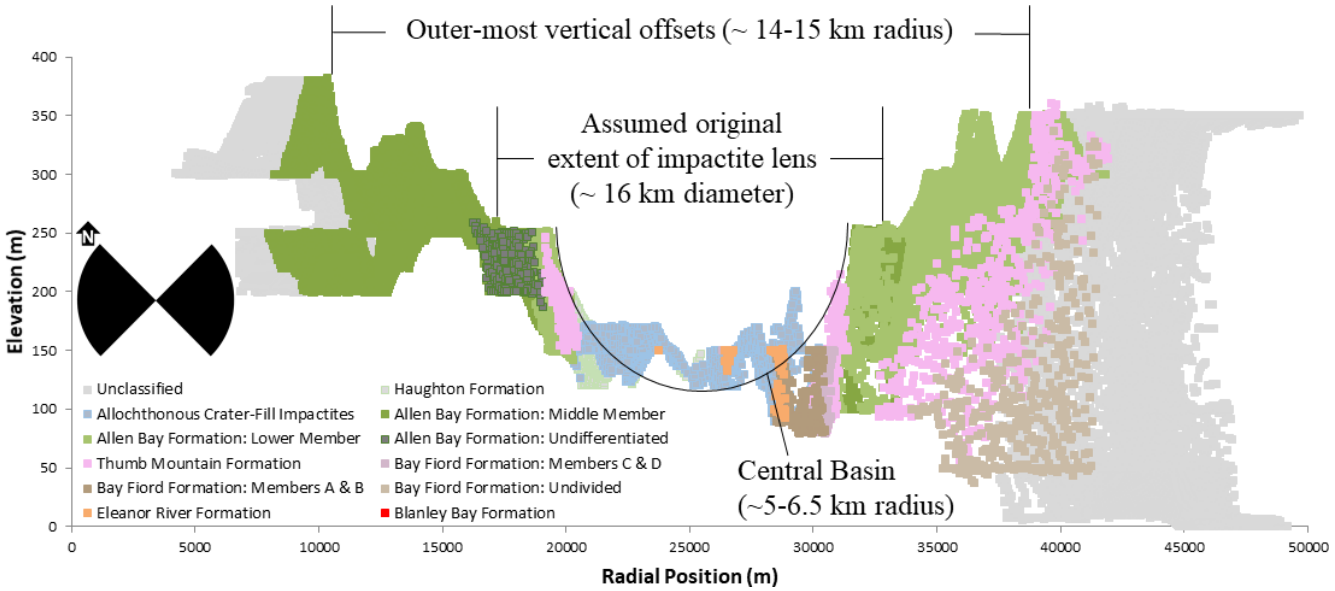

Fig. 4. This annotated pseudo cross section identifies some of the structural observations of the HIS that were made apparent by the new pseudo cross section method. Fm. = formation, Mt. = mountain, Lw. = lower. Elevation is above sea level. 50:1 vertical exaggeration. The diametrically opposed, black wedge shapes indicate the Cartesian orientation of the sampled areas.

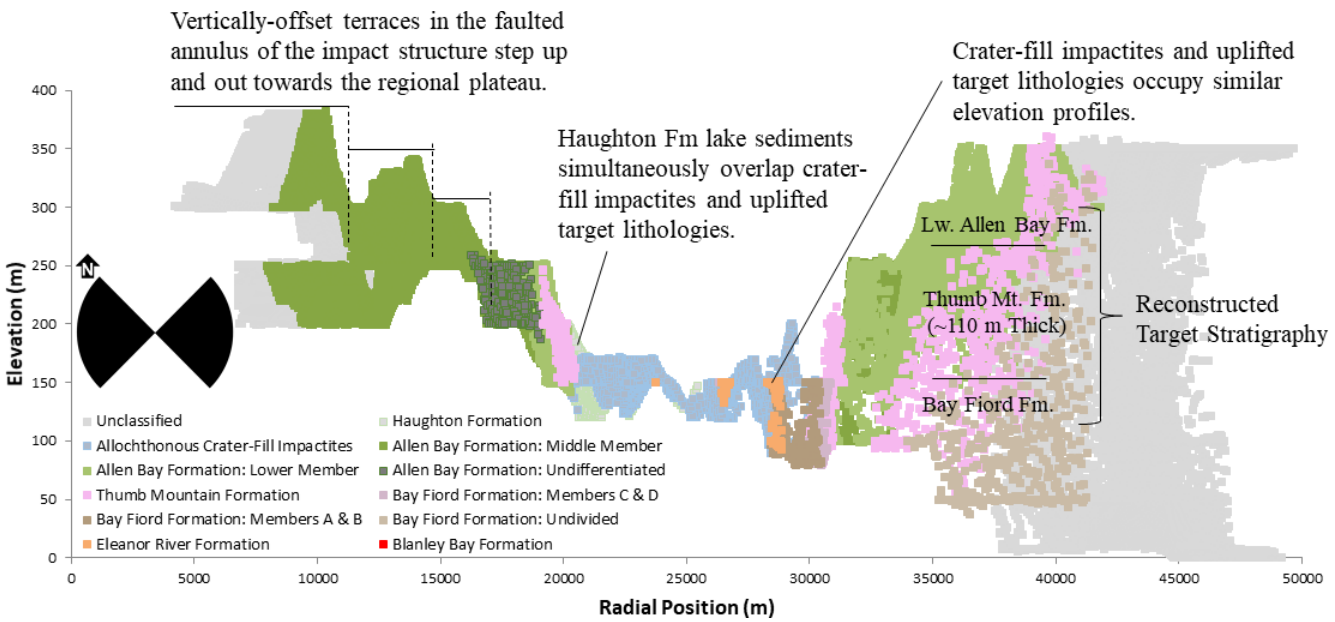

Fig. 5. This annotated pseudo cross section identifies additional structural observations of the HIS that were made apparent by the new pseudo cross section method. 50:1 vertical exaggeration. The diametrically opposed, black wedge shapes indicate the Cartesian orientation of the sampled areas.

valleys indicate the upper bound of erosion that this method can reconstruct. If the uneven elevation of the regional plateau surrounding the impact structure is a characteristic of the original target stratigraphy, it suggests that the magnitude of modification in the faulted annulus is at least partially related to the elevation of the target's surface. Specifically, quadrants of the faulted annulus that occupy lower surface elevations do not experience significant (>50 m) vertical shifts in the faults of the outer modified crater as far from the crater center as in quadrants that occupy higher surface elevations.

The pseudo sections successfully reconstruct a series of upward and outward stepping terraces. These terraces are bounded by offsets that rise up to the regional plateau at radial distances as great as 14–15 km to the northeast and southwest of the crater center (Fig. 5). For the most part, however, the terrace offsets reach the current regional plateau at radial distances between 11 and 12 km. In some cases, vertical offsets are observed in the reconstructed buried strata, with no surface expression in the form of a terrace (Fig. 5).

Central Basin

Within the HIS, the terraces step down toward the center of the impact structure, where a central basin with a radius between 5.0 and 6.5 km is observed in all of the pseudo cross sections (Fig. 4). It is important to note that the apparent steep-sided geometry displayed in these reconstructed sections is due to the large vertical exaggeration. In reality, the center of the HIS is a broad, shallow basin (~200–250 m deep), but the geometry is unique and consistent enough to be distinguished from the terraces of the outer region. The central basin contains all of the remaining allochthonous crater-fill impactites, as well as the Haughton Formation lake sediments, which are draped over the basin margins (Fig. 5). While the basin only contains uplifted target lithologies, between the margins of the central basin and innermost terrace offsets we observe both uplifted megablocks (i.e., Thumb Mountain and Bay Fiord formations) and downfaulted blocks that are not within the excavated crater (i.e., Allen Bay Formation).

Within the central basin, a series of observations unique to the 90° arc length wedge sections were made, due, in large part, to the juxtaposition of lithologies that are spatially separated by greater arc distances, but not by large geographic distances (Fig. 5). These observations include several examples of the Haughton Formation lake sediments overlapping both the impact target lithologies and the allochthonous crater-fill impactites, which are significant for interpreting the relative timing of postimpact erosional and depositional histories. There is also an interesting relationship between the elevation profiles of the allochthonous crater-fill impactites and the uplifted strata in the crater center (i.e., Eleanor River and Bay Fiord formations). The current elevation profiles of the crater-fill impactites and the target rocks of the central uplift are roughly equivalent, both maxing out at ~200 m above sea level. These units have undergone erosion down to similar elevations, which makes it difficult to determine which would have originally occupied a greater topographic rise.

DISCUSSION

A significant characteristic of the pseudo cross sections (90°, 45°, and 30°) is the difference in representational accuracy that different arc lengths of the wedges generate. Larger arc lengths (i.e., 90° wedge areas) sample larger spatial data sets that produce pseudo cross sections that appear more complete. However, in the distal components of these sections, geospatial data that are separated by the same arc lengths are also separated by relatively greater geographic distances. These data points are, thus, not as closely related spatially as data points plotted toward the center with the same or similar arc length separation. For identifying discrete structures within the study area, decreasing the angular range of the wedges ensures a closer spatial association of sampled data points in the distal portions of the impact structure. The larger area wedges can be used to summarize observations (see Figs. 4 and 5). Inner crater features are best identified using the larger arc length wedges, since the geographic distances become much smaller toward the center of the crater as the wedge areas converge. The best approach to analyzing the results is to scrutinize them individually and then seek out concurrency through observation of multiple wedges. Combining two of the three series, one with a large arc length (90°) and one with a smaller arc length (45° or 30°), was found to be most suitable for assessing the morphology of the impact structure. The 30° wedge areas provided results that were more distinctive than the 45° wedge areas, when compared to the 90° results. However, these results may vary depending on the field circumstances and the quality of geospatial data.

Central Basin

The most consistently observed structure derived from the pseudo cross sections is the steep-sided depression with a radius of 5–6.5 km at the center of the impact structure. This depression is bounded by uplifted target rocks (i.e., the Thumb Mountain, Bay Fiord, and Lower Allen Bay formations) that rise to an elevation of ~250 m above sea level, and punctured by uplifted outcrops of deeply excavated target material. When viewed without the vertical exaggeration produced in the cross sections, the steep-sided basin is in reality very broad, and shallow, and contains all outcrops of the Eleanor River and Blanley Bay formations, as well as the entire Haughton Formation deposit and the remnant allochthonous crater-fill impactite lens. The radial dimensions of the central basin are consistent with the transient cavity dimensions suggested by Osinski et al. (2005a), and the

stratigraphic makeup of the walls that form the edge of the basin is consistent with the description by these authors of uplifted (from 250 to 750 m deep), subvertical to overturned megablocks. Within the central basin, the intermediate uplift zone of megablocks from depths of ~ 1300 m is observed as mounds of the Eleanor River and Blanley Bay formations between radii of 1.0 and 5.0 km from the crater center. The central core of very deep uplifted material (~1450 m) was not observed, and in all sections, the 2.0 km diameter center area of the basin is entirely occupied by allochthonous crater-fill impactites (and some fluvial and glacial sediment deposits).

Postimpact Geological History

Within the central basin, Haughton Formation lake sediments were observed to simultaneously overlap both allochthonous crater-fill impactites and uplifted target strata such as the Bay Fiord and Eleanor River formations. This spatial relationship is significant, assuming that immediately after impact, the central basin was filled with a sheet of crater-fill melt rocks. In order for the lake sediments to have been deposited immediately overtop of both would require a period of significant erosion subsequent to the impact event and predating the deposition of lake sediments. Frisch and Thorsteinsson (1978) dated the lake sediments based on paleontological evidence as being Miocene in age, which is similar to geochronological ages determined by Omar et al. (1987) and Jessberger (1988) of 22.4 ± 1.4 Ma and 23.4 ± 1.0 Ma, respectively. They concluded that the Haughton Formation was deposited immediately after the initial formation of the impact structure. More recent geochronology by Young et al. (2013) indicates an Oligocene age of ~23.5 Ma. Haughton Formation sediments in the pseudo sections support a delayed deposition of the Miocene lake sediments—and, thus, indirectly the Oligocene or older (Sherlock et al. 2005) impact age determination for the Haughton impact event. This is also in agreement with Osinski and Lee (2005), who suggest that deposition of the Haughton Formation was delayed by 10^5–10^6 yr after the impact event.

Central Uplift

Within the central basin, the allochthonous crater-fill impactites and the uplifted target rocks have similar elevation profiles. The impactites rise in elevation to ~200 m above sea level, which constrains estimates of the minimum original elevation of the pre-erosional crater-fill lens. The target rocks that constitute the central uplift also rise to a similar maximum elevation in southern wedge areas and therefore likely share the same minimum pre-erosional elevation as the crater-fill. Osinski and Spray (2005) concluded that there was no original central peak structure on the basis that the central uplift did not originally protrude from the crater-fill lens. However, the observations made here using the pseudo cross section method do not require that interpretation, and it remains a possibility that there was originally a poorly formed peak structure or even a central peak ring, although there is little explicit evidence to support this conclusion. Nonetheless, the possibility of an original central peak structure cannot be dismissed based on elevation data.

Terraces and the Limit of Modification

Beyond the central basin, the pseudo cross sections provide excellent reconstructions of the upward- and outward-stepping series of terraces. These terraces are likely bounded by inward-dipping normal faults with vertical offsets of up to 50 m, and represent modification of the crater rim. The terraces typically reach the regional plateau (up to 350–380 m above sea level) between 11 and 12 km from the crater center, but sometimes offsets are observed as far as 14–15 km from the crater center (Fig. 4). To the northwest, there are no terraces observed beyond the central basin (see Fig. S1 in supporting information), and, in some of the sections, only a rim situated between 8 and 12 km from the crater center was observed. The outermost vertical offsets observed in the sections are largely consistent with the apparent crater diameter (~23 km) proposed by Osinski et al. (2005a), and the requirement of a semicontinuous circumferential normal faults, since no normal faulting beyond the 11–12 km radial distance was identified during field investigations. This interpretation is still largely predicated on a seismic section that crossed a normal fault at ~12 km from the crater center (Scott and Hajnal 1988), but the survey did not extend far beyond this radius and does not preclude the possibility of normal faults at greater distances. While the apparent crater diameter based on surface observations of the current erosional state of the impact structure might be ~23 km, the original extent of modification could be as great as 14–15 km from the crater center. However, normal faults at these distances have not been identified, so a greater extent of modification cannot be validated.

The innermost vertical offsets are consistently at ~ 8 km from the crater center, and rise to about 300 m above sea level. These innermost offsets form a nearly continuous ring around the structure that rises well above the central basin (which is assumed to have been

initially filled with the impactite lens) and its dimensions are consistent with the final crater rim interpreted by Osinski et al. (2005a, 2005b). However, in order for this rim to meet the requirements of the final crater, the allochthonous crater fill would have to exceed the bounds of the central basin (Grieve et al. 1981; Turtle et al. 2005), completely burying it, requiring an original maximum elevation to be greater than 250 m above sea level, and less than the elevation of the rim (i.e., less than 300 m above sea level). Given these requirements, it can be inferred that the original crater-fill impactite lens filled the basin up to elevations of 250–300 m, out to a radius of 8 km.

CONCLUSION

Through a novel new geomatics GIS pseudo cross section method involving the integration of geologic mapping and digital elevation models, and by sampling these data using a range of wedge-shaped areas, it was possible to plot diametrically opposed areas to produce representative pseudo cross sections of the HIS. This case study focused on structures associated with impact-related modification of the original target stratigraphy to assess the pre-erosional morphology of the impact structure. The results of the study, applied to previous structural interpretations by Osinski et al. (2005a), were largely conformable.

If this new methodology is applied to other impact structure studies, the display priority in developing pseudo cross sections (e.g., color scheme, stratigraphic units included, order of foreground lithologies in the graphic, and vertical exaggeration) should be adjusted to reflect the research goals of the study. The optimal application of the new GIS method is a combination of two series of different wedge areas (e.g., 90° and 30° series). Inclusion of a third intermediate series (e.g., 45°) was determined to be largely redundant, with more distinct results being derived from the 30° series. The 30° wedge area series was useful for identifying discrete features in the distal components of the impact structure with a higher degree of certainty regarding their spatial relationship. The 90° wedge area series was most useful for identifying features in the structure interior and for summarizing observations made in the smaller 30° series.

Overall, this new GIS-based pseudo cross section method effectively reproduces important impact-related structures described by Osinski et al. (2005a) and provides useful ancillary information about the HIS. It is, thus, a useful adjunct to high quality, detailed mapping, with the capacity to add additional constraints on qualitative and quantitative conclusions.

Acknowledgments—This research on the HIS was initiated during a summer internship at the Lunar and Planetary Institute, Houston, carried out under the supervision of Dr. Virgil "Buck" Sharpton, and funded by the Undergraduate Science Research Association. The research was subsequently supported by the mentorship, guidance (and editorial services) of Dr. Tim Patterson and Dr. Elizabeth Anderson.

Editorial Handling—Dr. Gordon Osinski

REFERENCES

Bischoff L. and Oskierski W. 1988. The surface structure of the Haughton impact structure, Devon Island, Canada. *Meteoritics* 23:209–220.

Dence M. R. 1965. The extraterrestrial origin of Canadian craters. *Annals of the New York Academy of Science* 123:941–969.

Dence M. R. 1972. The nature and significance of terrestrial impact structures. Proceedings, 15th International Geological Congress. pp. 77–89.

Frisch T. and Thorsteinsson R. 1978. Haughton astrobleme: A midCenozoic impact crater, Devon Island, Canadian Arctic Archipelago. *Arctic* 31:108–124.

Government of Canada. n.d. Geospatial data extraction. https://maps.canada.ca/czs/index-en.html. Accessed January 2, 2019.

Greenberger R. N., Mustard J. F., Osinski G. R., Tornabene L. L., Pontefract A. J., Marion C. L., Flemming R. L., Wilson J. H., and Cloutis E. A. 2016. Hyperspectral mapping of alteration assemblages within a hydrothermal vug at the Haughton impact structure, Canada. *Meteoritics & Planetary Science* 51:2274–2292.

Greiner H. R. 1963. Haughton Dome and area southwest of Thomas Lee Inlet. In *Geology of the north–central part of the Arctic Archipelago, Northwest Territories (Operation Franklin)*, Geological Survey of Canada Memoir 320, edited by Fortier Y. O., Blackadar R. G., Glenister B. F., Greiner H. R., McLaren D. J., McMillan N. J., Norris A. W., Roots E. F., Souther J. G., and Thorsteinsson R. Ottawa: Geological Survey of Canada. pp. 208–216.

Grieve R. A. F. 1981. Impact cratering. *Nature* 291:16.

Grieve R. A. F. 1988. The Haughton impact structure: Summary and synthesis of the results of the HISS project. *Meteoritics* 23:249–254.

Grieve R. A. F., Robertson P. B., and Dence M. R. 1981. Constraints on the formation of ring impact structures, based on terrestrial data. In *Proceedings of the conference on multi-ring basins: Formation and evolution*, edited by Schultz P. H. and Merrill R. B. New York: Pergamon Press. pp. 37–57.

Hajnal Z., Scott D., and Robertson P. B. 1988. Reflection study of the Haughton impact crater. *Journal of Geophysical Research* 93:11,930–11,942.

Hickey L. J., Johnson K. R., and Dawson M. R. 1988. The stratigraphy, sedimentology, and fossils of the Haughton Formation: A post impact crater-fill. *Meteoritics* 23:221–231.

Izawa M. R. M., Banerjee N. R., Osinski G. R., Flemming R. L., Parnell J., and Cockell C. S. 2011. Weathering of post-impact hydrothermal deposits from the Haughton impact

structure: Implication for microbial colonization and biosignature preservation. *Astrobiology* 11:537–550.

Jessberger E. K. 1988. $^{40}Ar/^{39}Ar$ dating of the Haughton impact structure. *Meteoritics* 23:233–234.

Kenkmann T., Jahn A., Scherler D., and Ivanov B. A. 2005. Structure and formation of a central uplift: A case study at the Upheaval Dome impact crater, Utah. In *Large meteorite impacts III*, edited by Kenkmann T., Hörz F., and Deutsch A. GSA Special Paper #384. Boulder, Colorado: Geological Society of America. pp. 85–115.

Lee P., Bunch T. E., Cabrol N., Cockell C. S., Grieve R. A. F., McKay C. P., Rice J. W. J., and Schutt J. W. 1998. Haughton–Mars 97–I: Overview of observations at the Haughton impact crater, a unique Mars analog site in the Canadian High Arctic (abstract #1973). 29th Lunar and Planetary Science Conference. CD-ROM.

Metzler A., Ostertag R., Redeker H. J., and Stöffler D. 1988. Composition of the crystalline basement and shock metamorphism of crystalline and sedimentary target rocks at the Haughton impact crater, Devon Island, Canada. *Meteoritics* 23:197–207.

Omar G., Johnson K. R., Hickey L. J., Robertson P. B., Dawson M. R., and Barnosky C. W. 1987. Fission-track dating of Haughton astrobleme and included biota, Devon Island, Canada. *Science* 237:1603–1605.

Osinski G. R. 2005. Geological map Haughton impact structure Devon Island, Nunavut, Canada. *Supplement to Meteoritics & Planetary Science* 40(12).

Osinski G. R. and Ferrière L. 2016. Shatter cones: (Mis) understood? *Science Advances* 2:e1600616.

Osinski G. R. and Lee P. 2005. Intra-crater sedimentary deposits at the Haughton impact structure, Devon Island, Canadian High Arctic. *Meteoritics & Planetary Science* 40:1887–1899.

Osinski G. R. and Spray J. G. 2005. Tectonics of complex crater formation as revealed by the Haughton impact structure, Devon Island, Canadian High Arctic. *Meteoritics & Planetary Science* 40:1789–1812.

Osinski G. R., Lee P., Spray J. G., Parnell L. D., Bunch T. E., Cockell C. S., and Glass B. 2005a. Geological overview and cratering model for the Haughton impact structure, Devon Island, Canadian High Arctic. *Meteoritics & Planetary Science* 40:1759–1776.

Osinski G. R., Spray J. G., and Lee P. 2005b. Impactites of the Haughton impact structure, Devon Island, Canadian High Arctic. *Meteoritics & Planetary Science* 40:1789–1812.

Parnell J., Lee P., Cockell C. S., and Osinski G. R. 2004. Microbial colonization in impact-generated hydrothermal sulphate deposits, Haughton impact structure, and implication for sulphates on Mars. *International Journal of Astrobiology* 3:247–256.

Pohl J., Eckstaller A., and Robertson P. B. 1988. Gravity and magnetic investigations in the Haughton impact structure, Devon Island, Canada. *Meteoritics* 23:235–238.

Quesnel Y., Gattacceca J., Osinski G. R., and Rochette P. 2013. Origin of the central magnetic anomaly at the Haughton impact structure, Canada. *Earth and Planetary Science Letters* 367:116–122.

Redeker H. J. and Stöffler D. 1988. The allochthonous polymict breccia layer of the Haughton impact crater, Devon Island, Canada. *Meteoritics* 23:185–196.

Robertson P. B. 1988. The Haughton impact structure, Devon Island, Canada: Setting and history of investigations. *Meteoritics* 13:615–618.

Robertson P. B. and Grieve R. A. F. 1978. The Haughton impact structure. *Meteoritics* 13:615–618.

Robertson P. B. and Mason G. D. 1975. Shatter cones from Haughton Dome, Devon Island, Canada. *Nature* 255:393–394.

Robertson P. B. and Plant A. G. 1981. Shock metamorphism in sillimanite from the Haughton impact structure, Devon Island, Canada. *Contributions to Mineralogy and Petrology* 78:12–20.

Robertson P. B. and Sweeney J. F. 1983. Haughton impact structure: Structural and morphological aspects. *Canadian Journal of Earth Sciences* 20:1134–1151.

Scott D. and Hajnal Z. 1988. Seismic signature of the Haughton structure. *Meteoritics* 23:239–247.

Sharpton V. L. 1999. The nature of central peak rings: Evidence from the Haughton crater (abstract). *Meteoritics & Planetary Science* 34:A107.

Sharpton V. L., Dressler B. O., and Sharpton T. J. 1998. Mapping the Haughton impact crater, Devon Island, NWT; implications for the shape and size of the excavation cavity (abstract #1867). 29th Lunar and Planetary Science Conference. CD-ROM.

Sherlock S. C., Kelley S. P., Parnell J., Green P., Lee P., Osinski G. R., and Cockell C. S. 2005. Re-evaluating the age of the Haughton impact event. *Meteoritics & Planetary Science* 40:1777–1787.

Thorsteinsson R. and Mayr U. 1987. *The sedimentary rocks of Devon Island, Canadian Arctic Archipelago, Geological Survey of Canada Memoir #411*. Ottawa: Geological Survey of Canada. 182 p.

Tobler W. 1970. A computer movie simulating urban growth in the Detroit region. *Economic Geography* 46(Suppl.):234–240.

Todd F. J. 1979. *Gravity study of Haughton dome, Devon Island, Northwest Territories*. B.Sc. thesis, University of Western Ontario, London, Ontario, Canada. 68 p.

Turtle E. P., Pierazzo E., Collins G. S., Osinski G. R., Melosh H. J., Morgan J. V., Reimold W. U., and Spray J. G. 2005. Impact structures: What does crater diameter mean? In *Large meteorite impacts III*, edited by Kenkmann T., Hörz F., and Deutsch A. GSA Special Paper #384. Boulder, Colorado: Geological Society of America. pp. 1–24.

Young K. E., van Soest M. C., Hodges K. V., Watson E. B., Adams B. A., Lee P. 2013. Impact thermochronology and the age of haughton impact structure, Canada. *Geophysical Research Letters* 40:3836–3840.

Zent A. P., Bunch T. E., Lee P., Rice J. W. J., McKay C. P., Schutt J. W., and Grieve R. A. F. 1998. The role of brecciation in controlling morphology at Haughton crater: Climatic implications for Mars (abstract #1301). 29th Lunar and Planetary Science Conference. CD-ROM.

Zylberman W., Quesnel Y., Rochette P., Osinski G. R., Marion C., and Gattacceca J. 2017. Hydrothermally-enhanced magnetization at the center of the Haughton impact structure? *Meteoritics & Planetary Science* 52:2147–2165.

SUPPORTING INFORMATION

Additional supporting information may be found in the online version of this article.

Fig. S1. A) This northwest to southeast oriented pseudo cross section (50× vertical exaggeration) was constructed from diametrically opposed 90° wedge areas (lower left corner of plot area) with angular positions with respect to the crater center between north and N90°W for the northwest wedge area (left of 25,000 m), and between south and S90°E for the southeast wedge area (right of 25 000 m). 50:1 vertical exaggeration.

B) This southwest to northeast oriented pseudo cross section (50× vertical exaggeration) was constructed from diametrically opposed 90° wedge areas (lower left corner of plot area) with angular positions with respect to the crater center between south and S90°W for the southwest wedge area (left of 25,000 m), and between north and N90°E for the northeast wedge area (right of 25,000 m). 50:1 vertical exaggeration.

C) This north–northwest to south–southeast oriented pseudo cross section (50× vertical exaggeration) was constructed from diametrically opposed 45° wedge areas (lower left corner of plot area) with angular positions with respect to the crater center between north and N45°W for the north–northwest wedge area (left of 25,000 m), and between south and S45°E for the south–southeast wedge area (right of 25,000 m). 50:1 vertical exaggeration.

D) This west–northwest to east–southeast oriented pseudo cross section (50× vertical exaggeration) was constructed from diametrically opposed 45° wedge areas (lower left corner of plot area) with angular positions with respect to the crater center between west and N45°W for the west–northwest wedge area (left of 25,000 m), and between east and S45°E for the east–southeast wedge area (right of 25,000 m). 50:1 vertical exaggeration.

E) This west–southwest to east–northeast oriented pseudo cross section (50× vertical exaggeration) was constructed from diametrically opposed 45° wedge areas (lower left corner of plot area) with angular positions with respect to the crater center between west and S45°W for the west–southwest wedge area (left of 25,000 m), and between east and N45°E for the east–northeast wedge area (right of 25,000 m). 50:1 vertical exaggeration.

F) This south–southwest to north–northeast oriented pseudo cross section (50× vertical exaggeration) was constructed from diametrically opposed 45° wedge areas (lower left corner of plot area) with angular positions with respect to the crater center between south and S45°W for the south–southwest wedge area (left of 25,000 m), and between north and N45°E for the north–northeast wedge area (right of 25,000 m). 50:1 vertical exaggeration.

G) This north–northwest to south–southeast oriented pseudo cross section (50× vertical exaggeration) was constructed from diametrically opposed 30° wedge areas (lower left corner of plot area) with angular positions with respect to the crater center between north and N30°W for the north–northwest wedge area (left of 25,000 m), and between south and S30°E for the south–southeast wedge area (right of 25,000 m). 50:1 vertical exaggeration.

H) This northwest to southeast oriented pseudo cross section (50× vertical exaggeration) was constructed from diametrically opposed 30° wedge areas (lower left corner of plot area) with angular positions with respect to the crater center between N60°W and N30°W for the northwest wedge area (left of 25,000 m), and between S60°E and S30°E for the southeast wedge area (right of 25,000 m). 50:1 vertical exaggeration.

I) This west–northwest to east–southeast oriented pseudo cross section (50× vertical exaggeration) was constructed from diametrically opposed 30° wedge areas (lower left corner of plot area) with angular positions with respect to the crater center between N60°W and west for the west–northwest wedge area (left of 25,000 m), and between S60°E and east for the east–southeast wedge area (right of 25,000 m). 50:1 vertical exaggeration.

J) This west–southwest to east–northeast oriented pseudo cross section (50× vertical exaggeration) was constructed from diametrically opposed 30° wedge areas (lower left corner of plot area) with angular positions with respect to the crater center between S60°W and west for the west–southwest wedge area (left of 25,000 m), and between N60°E and east for the east–northeast wedge area (right of 25,000 m). 50:1 vertical exaggeration.

K) This southwest to northeast oriented pseudo cross section (50× vertical exaggeration) was constructed from diametrically opposed 30° wedge areas (lower left corner of plot area) with angular positions with respect to the crater center between S60°W and S30°W for the southwest wedge area (left of 25,000 m), and between N60°E and N30°E for the northeast wedge area (right of 25,000 m). 50:1 vertical exaggeration.

L) This south–southwest to north–northeast oriented pseudo cross section (50× vertical exaggeration) was constructed from diametrically opposed 30° wedge (lower left corner of plot area) areas with angular positions with respect to the crater center between south and S30°W for the south–southwest wedge area (left of 25,000 m), and between north and N30°E for the north–northeast wedge area (right of 25,000 m). 50:1 vertical exaggeration.